Thermodynamic properties of minerals and fluids

Khodorevskaya L.I., Kosova S.A., Viryus A.A. Melt compositions during partial melting of gabbro-anorthosites under conditions of chemical potential gradients of FeO, V_2O_3 and TiO_2. *UDC 552.13*

D.S. Korzhinskii Institute of Experimental Mineralogy the Russian Academy of Sciences (IEM RAS), Chernogolovka Moscow district. khodorevskaya@mail.ru

Abstract. In the studies (Khodorevskaya et al., article in this collection) an experimental study was conducted on the interaction of gabbro-anorthosites with H_2O-NaCl and H_2O - NaCl - CO_2 fluids at T = 900 °C, P = 5 kbar under equilibrium conditions. This article presents the compositions of melts formed during partial melting of anorthosite under nonequilibrium conditions that ensure the input-output of elements.

Introduction. The studies (Bogdanova et al. 1993; Fonarev, Konilov, 2005, Khodorevskaya, Korikovskii, 2007) showed that at the peak of Svecofennian metamorphism and its retrograde stage in the gabbro-anorthosites of the Kolvitsky massif, conditions were created for filtration of deep fluids of various compositions through the massif. The elements removed by the fluids were redeposited in the form of melanocratic metasomatic veins enriched in mafic and ore components. A detailed description of the vein thickness, zoning, mineral compositions, and formation parameters is presented in (Khodorevskaya, 2012). The results of an experimental study of the interaction of gabbro-anorthosites with H_2O-NaCl and H_2O - NaCl - CO_2 fluids at T = 900 °C, P = 5 kbar under stationary conditions are described in (Khodorevskaya et al., article in this collection). A disadvantage of such experiments from the standpoint of the formation of metasomatic associations is the absence of any gradients (e.g., temperature, pressure, etc.), which are the driving forces of component transfer by fluids. In this work, we attempted to reproduce the transfer of components under conditions of chemical potential gradients of FeO, V_2O_3 and TiO_2.

Technique and methodology of experiments. The chemical and mineral composition of the initial gabbro-anorthosite is presented in (Khodorevskaya et al., article in this collection). The experiments were carried out using a two-ampoule technique (Fig. 1) in high gas pressure setups at 900°C and 500 MPa. 25–40 mg of anorthosite (2 in Fig. 1), pre-mixed with 3–5% TiO_2, FeO, and V_2O_3, was placed into the inner, vertically located ampoule with a diameter of 5 mm and a height of 50 mm (1 in Fig. 1). H_2O + NaCl were added to the ampoule (Table 1, 3 in Fig. 1). Then the outer ampoule was squeezed at a distance of ≈ 20 mm from the top, and a small ampoule (4 in Fig. 1) with a diameter of 3 mm and a height of 10–15 mm was placed into it. A small ampoule also contained a sample of anorthosite, but without the addition of TiO_2, FeO, V_2O_3 (5 in Fig. 1). This ampoule was compressed both from the sides and at the top, but was not welded; the outer ampoule was welded. Thus, it was assumed that the anorthosite in the large ampoule represented the host rock from which the components were carried out by the fluid and redeposited in the small (inner ampoule) due to the gradients of chemical potentials (oxide masses), as well as some pressure gradients in the outer and inner, initially compressed ampoule. V_2O_3, which was in the anorthosite sample in the outer ampoule (2 in Fig. 1), but was not in the inner ampoule (5 in Fig. 1), served as an indicator of the transfer of components by the fluid. The transfer of elements occurred until equilibrium was established in the outer and inner ampoules. Complete identity of the mineral composition in the outer and inner ampoules and their identical chemical composition indicated the onset of equilibrium, while the unequal composition of the phases meant the absence of equilibrium in the system due to gradient conditions. Accordingly, the duration of the experiments and the composition of the fluid phase were important for the transfer of components. In the experiments lasting 7 days, almost complete equilibrium was observed in the outer and inner ampoules, while in 4 days, complete equilibrium did not occur in any of the experiments.

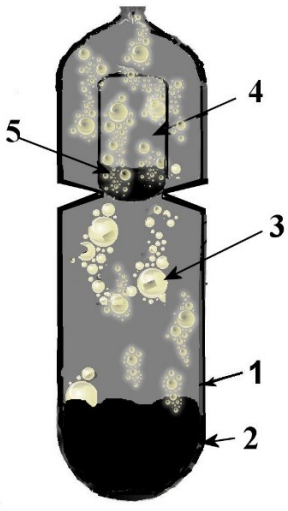

Fig. 1. Experimental scheme. 1 – outer ampoule, 2 – anorthosite sample + 3-5% TiO_2, FeO, V_2O_3, 3 – initial solution H_2O+NaCl, 4 – inner ampoule, 5 – anorthosite sample without added TiO_2, FeO, V_2O_3.

Experimental results. Table 1 shows the compositions of the fluid phase and the main mineral associations after the experiments. For the given parameters, amphibole and quenched melt are the main phases after the experiments regardless of the fluid composition (Fig. 2). In the small ampoule of experiment B-X, long, up to 200 μm, very thin orthoamphibole needles appear, clearly visible to the

naked eye, while in the other large and small ampoules, amphibole is represented by Ca-amphibole plates. Clino- and orthopyroxenes were not detected in the experiments with low salt contents (experiment 5-IS). With an increase in the salinity of the solutions (experiment A-X), pyroxenes are preserved only in the form of remaining small grains surrounded by amphibole (Fig. 1a), i.e. they also become unstable. In experiment E-X, clinopyroxenes are large, without traces of corrosion. The zoned plagioclase from An58 in the center to An25-35 is preserved in both the large and small ampoules only in the experiments with a high salt content (experiment E-X). Fig. 2 shows that complete identity of the phases after experiments in the large and small ampoules is achieved only in experiment E-X.

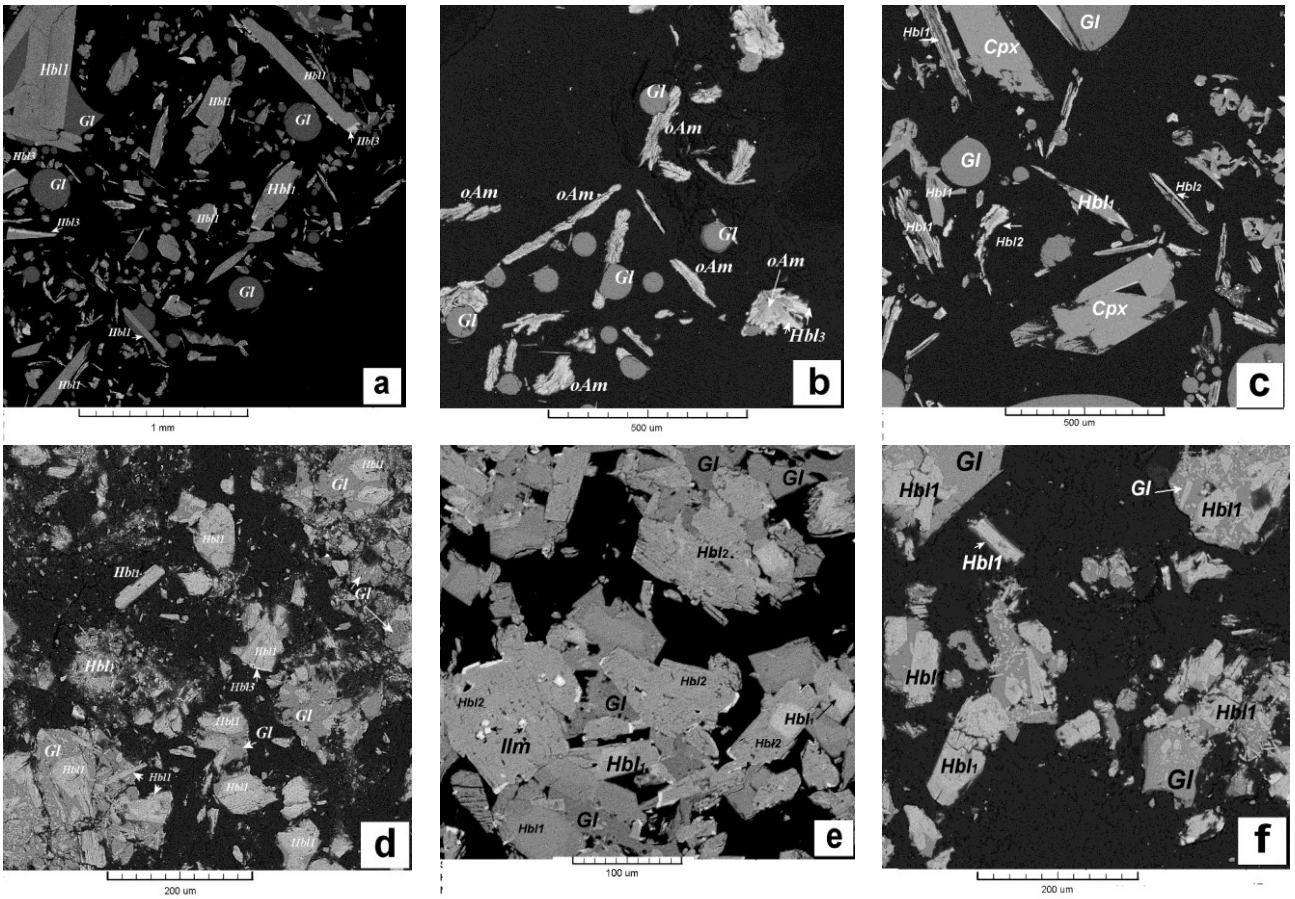

Fig. 2. Photographs of the products of backscattered electron (BSE) experiments. (a) – experiment B-X, outer ampoule: amphibole (Hbl1) and quenched melt (Gl), (b) – experiment B-X, inner ampoule: orthoamphibole (oAm) and melt Gl; (c-d) – experiment A-X, outer and inner ampoules, (d-f) – experiment E-X, outer and inner ampoules.

Table 1. Composition of the initial fluid in the ampoules and phase associations after the experiments

№	Duration of experiments, hours.	Composition of the fluid	Phases after the experiment	
			Large ampoule	Small ampoule
B-X	96	$X_{NaCl} = 0.15$ $X_{H2O} = 0.66$	*Gl+Hbl$_1$+Hbl$_2$*	*Gl+oAm+ Hbl$_2$*
A-X	96	$X_{NaCl} = 0.34$ $X_{H2O} = 0.85$	*Gl+Hbl$_1$+Cpx+ Hbl$_2$*	*Gl+Hbl$_1$+ Hbl$_2$*
E-X	96	$X_{NaCl} = 0.49$ $X_{H2O} = 0.51$	*Gl+Hbl$_1$+Cpx+ Hbl$_2$+Pl+Ilm*	*Gl+Hbl$_1$+ Hbl$_2$ +Cpx + Pl*
1	168	0	*Gl+Hbl$_1$+Ilm±Pl*	*Gl+Hbl$_1$+Pl*
2	168	$X_{NaCl} = 0.06$ $X_{H2O} = 0.94$	*Gl+Hbl$_1$+Hbl$_2$+Pl+Rt*	*Gl+Hbl$_1$ +Hbl$_2$+Pl*
4	168	$X_{NaCl} = 0.07$ $X_{H2O} = 0.51$ + graphite	*Gl+Hbl$_1$+Hbl$_2$+Pl+Rt*	*Gl+Hbl$_1$+Hbl$_2$+Pl*
5	168	$X_{NaCl} = 0.18$ $X_{H2O} = 0.41$ $X_{CO2} = 0.41$	*Gl+Hbl$_1$+Hbl$_2$+Rt+Opx*	*Gl+Hbl$_1$+ Hbl$_2$+Rt±Opx*

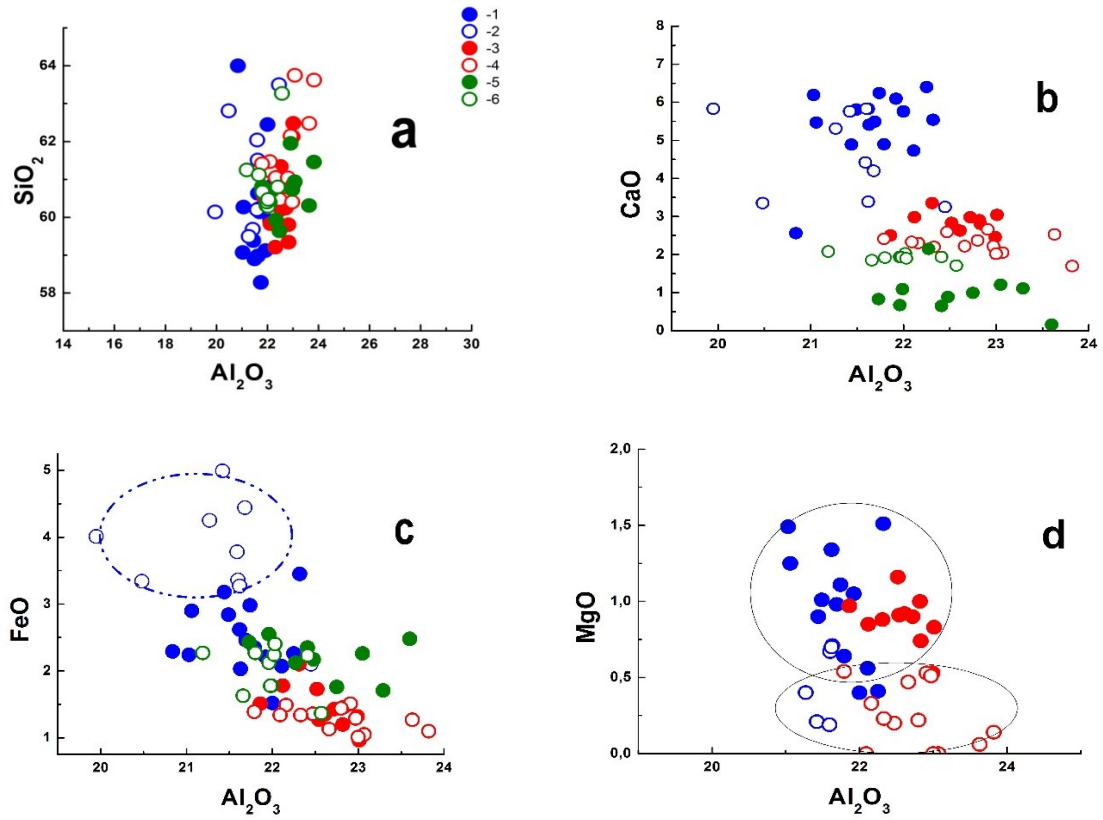

Fig. 3. The ratio of oxides in melts. Legend here and in Fig. 4: 1, 3, 5 – in large ampoules of experiments B-X, A-X, E-X respectively, 2, 4, 6 – in small ampoules of the same experiments

Quenching melts. In Fig. 3a-g, the ratio of oxides in the large and small ampoules in experiments B-X, A-X and E-X is shown with colored symbols.

The Al_2O_3 content is the same in both the outer and inner ampoules in all experiments and corresponds to equilibrium values of ≈ 22.5 ±1.5 wt. % (Fig. 3a). Such small variations in Al_2O_3 in the fluid allow us to consider changes in the content of components such as CaO, FeO and others relative to the almost constant values of Al_2O_3.

CaO content. In experiments B-X and A-X, the CaO content in melts from the large (blue and red filled circles in Fig. 3b) and small ampoules (blue and red hollow circles in Fig. 3b) is close to equilibrium. In experiment E-X, the CaO content in melts from the large ampoule is lower than in melts from the small ampoule, indicating a nonequilibrium distribution of Ca during the experiments. In general, with an increase in X_{NaCl} in the fluid filtering through the rock, increasingly sodium-rich melts are formed and Ca is removed from the host rocks.

FeO content. The FeO content in the melts from the large and small ampoules in both experiment A-X and experiment E-X is practically the same (red and green circles in Fig. 3c), i.e. equilibrium is established in the system. At the same time, with an increase in X_{NaCl} in the fluid filtering through the rock from 0.34 to 0.49, increasingly more ferruginous melts are formed. In experiment B-X, the FeO content in the melt from the small ampoule is higher (the outlined field in Fig. 3c) than in the large ampoule; FeO is carried out of the large ampoule.

MgO content. In the B-X and A-X experiments, the MgO content in the melts from the large ampoules is practically the same (Fig. 4b) and is higher than in the small ampoules, i.e. MgO is not removed from the large ampoule, and equilibrium does not occur. In the E-X experiment, the MgO content in the melts from the large and small ampoules is practically the same, at a level of ≈ 0.5 wt.%.

V_2O_3 in the melts is very small, no more than 0.3%, TiO_2 no more than 0.6% and is practically independent of X_{NaCl} in the fluid.

Amphiboles. In all the experiments, Ca-amphibole *Hbl₁* is the main mineral and belongs to pargasite. In the margins of some *Hbl₁*, ferrous amphibole *Hbl₃* appears. The high NaCl content in the initial fluid leads to the formation of *Hbl₂*, which develops along the edges of *Hbl₁* (Fig. 2d). *Hbl₂* is characterized by an intermediate composition between pargasite and richterite. In addition, in the B-X experiment, orthoamphibole, rather than Ca-amphibole, is formed in a small ampoule. Its average composition is

$(Na_{0.95}K_{0.06})_{1.01}(Na_{0.48}Ca_{0.28}Fe^{2+}_{1.21})_2(Mg_{1.47}Fe^{2+}_{2.04}Fe^{3+}_{0.81}Ti_{0.08}Al_{0.6})_5(Si_{6.16}Al_{1.84})O_{22}(OH)_2$, close to ferrogedrite, iron content f ≈0.75.

Clinopyroxenes are noted in experiments A-X and E-X, in which X_{H2O} is low. This is a mineral with low iron content (f= 0 – 0.10) and high (up to 14 wt.%) jadeite content.

Conclusion. Thus, the presented experiments showed that in experiments lasting 4 days, the equilibrium content of petrogenic components is not always established, which allows us to judge the input-output of components by the fluid phase. At relatively low X_{NaCl} in the fluid (X_{NaCl} = 0.15), Fe is removed from the anorthosite sample located in the large ampoule (the host rock according to the experiment model). This leads to the formation of relatively ferruginous melts with a high Ca content (Fig. 3b-c) and ferruginous orthoamphiboles. With an increase in X_{NaCl} in the fluid (experiments A-X and E-X), Fe equilibrium is noted in the large and small ampoules. Therefore, it is incorrect to judge the predominant Fe removal from the host rocks, although the low Fe contents in the melts from these experiments indicate that the Fe removal from the host rocks will decrease with an increase in fluid salinity.

At high X_{NaCl} in the fluid (X_{NaCl} = 0.34), on the contrary, the removal of Ca from the host rocks and the formation of increasingly sodium melts are observed. Mg, even with significant variations in X_{NaCl} in the fluid (from 0.15 to 0.34), is practically not removed from the host rocks. The Cl content in the melt increases with the growth of X_{NaCl} in the fluid from 0.90 to 1.5 wt.%, the chlorine content values in the large and small ampoules for each experiment are close. The content of V_2O_3 and TiO_2 in the melts is very small (0.3 and 0.6 wt.%, respectively) and practically does not depend on X_{NaCl} in the fluid, which does not allow us to judge the input-output of these components.

With a duration of experiments of 8 days, a complete equilibrium of elements in the large and small ampoules is established for each experiment.

Funding. The work was carried out within the framework of the research project of the IEM RAS No. FMUF-2022-0004.

References

Bogdanova M. N., Efimov M. M., Sorokhtin R. O., et al., Development of the Polymetamorphism in the Granulite Belt of the Kola Peninsula (Kolvitsa Zone), and U–Pb Dating the Diaphthoresis of the Anorthosite Association// Dokl. Akad. Nauk. 1993. V. 331. № 1. P. 95–98.

Fonarev V. I., Konilov A. N. Pulsating evolution of metamorphism in granulite terrains: Kolvitsa meta-anorthosite massif, Kolvitsa Belt, Northeast Baltic Shield //International Geology Review. 2005. T. 47. №. 8. C. 815-850.

Khodorevskaya L.I. Granulite facies metamorphism and metasomatism in the gabbro-anorthosites of the Kolvitsa massif, Kola peninsula// Geochemistry International. 2012. V. 50, № 3. P. 272-288.

Khodorevskaya L. I., Korikovskii S. P. Metasomatic Garnet–Clinopyroxene–Orthopyroxene–Hornblende Veins in Metaanorthosites of the Kolvitsa Massif, Kola Peninsula: Mineral Composition and Relation with Syngranulite Granitization //Dokl. Earth Sci. 2007. V. 415A. P. 915–918.

Khodorevskaya L.I., Kosova S.A., Viryus A.A. Partial melting of gabbro-anorthosites and concomitant metasomatosis with different composition of the fluid phase. Experimental studies. *UDC 552.13*

D.S. Korzhinskii Institute of Experimental Mineralogy the Russian Academy of Sciences (IEM RAS), Chernogolovka Moscow district. khodorevskaya@mail.ru

Abstract. In the gabbro-anorthosite complexes of the Belomorian complex at the peak of Svecofennian metamorphism there are metasomatic melanocratic veins associated with the removal of Ca, Fe, sometimes Mg, Ti from the host rocks. Experimental studies modeling metasomatic transformations of anorthosites during infiltration metasomatism are absent. This paper presents the results of the interaction of gabbro-anorthosites with H_2O-NaCl and H_2O - NaCl - CO_2 fluids at T = 900°C, P = 5 kbar under stationary conditions, i.e., without creating conditions for the transfer of elements by solutions. At the given parameters, partial melting of the rock occurs with the formation of acid plagioclase-normative melt, pargasite amphibole, carbonates. Diffusion of elements in minerals is manifested in the formation of extremely ferruginous compositions of the marginal parts of amphibole, a decrease in the Fe content in ilmenite, and the inclusion of Fe in the melt. The removal of Ti from anorthosite minerals is confirmed by its absence in the marginal parts of mafic anorthosite minerals. Mg was fixed in the marginal parts of amphibole or in chlorite. Localized formations of Fe-Ti minerals similar to ilmenite-magnetite deposits in natural melanocratic veins were not obtained in experiments.

Keywords: *garnet-two-micas schist, dehydration melting, graphite, granitoid melts, carbon dioxide fluid, inclusions, Raman spectra, experiment.*

Introduction. In the southwestern part of the Kolvitsky massif of layered gabbro-anorthosites (Belomorsky complex), thin melanocratic veins are observed, ranging from thin layered veinlets 0.5–12 cm wide to interlayers reaching 50 cm. Studies (Bogdanova et al. 1993; Korikovsky, Aranovich, 2010, etc.) have shown that due to the heterogeneity of the massif at the peak of Svecofennian metamorphism and its retrograde stage, conditions

were created for the filtration of deep fluids of various compositions through the massif, causing both local partial melting of rocks, including gabbro-anorthosites, and their metasomatic changes with the conversion of a number of elements into fluids.

The removed elements were redeposited in the massif in the form of melanocratic metasomatic veins enriched in mafic minerals (garnets, pyroxenes, amphiboles) and ore components (ilmenite, magnetite, sulfides). The formation of such veins in the anorthosites of the Kolvitsky massifs occurred at the parameters t = 910–750°C, P = 14–7 kbar with the participation of Fe, CO_2, Si, Na-containing solutions with low aH_2O (Khodorevskaya, 2012).

There are no targeted experimental studies modeling the metasomatic transformations of anorthosites during their partial melting under the influence of fluids of different compositions, although the conditions for the formation of Mag-Ilm internal zones in metasomatic veins are very important from the standpoint of the formation of magnetite-ilmenite ore occurrences. This paper presents the first results of an experimental test of the possibility of forming metasomatic associations during the interaction of anorthosites with single-phase (H_2O-NaCl) and two-phase fluid (H_2O-NaCl-CO_2).

Technique and methodology of experiments. A sample of anorthosites from the Kolvitsky massif was used as the initial rock. The chemical composition of anorthosites (wt.%): SiO_2 – 50.28, TiO_2 – 0.38, Al_2O_3 – 20.40, FeO – 6.74, MnO –0.25, MgO – 6.64, CaO – 12.21, Na_2O – 2.54, K_2O – 0.26, P_2O_5 – 0.18. Sometimes ≈ 3-5% TiO_2, FeO and V_2O_3 were added to the initial anorthosite sample. The main minerals of anorthosite are orthopyroxene ($En_{68.5}Fs_{31.5}$), clinopyroxene ($En_{40}Wo_{46-48}Fs_{11-13}$), plagioclase ($An_{98-100}$), and the following ore minerals are found: magnetite, ilmenite – ($Ilm_{0.90}Hem_{0.04}Gk_{0.04}$), $(Fe,Ni)_9S_8$, FeS, $CuFeS_2$, rutile (*Rt)*.

The experiments were carried out on high gas (Ar) pressure units with internal heating at 900°C and 500 MPa. A vertically located ampoule (5 mm in diameter and 50 mm in height) was successively filled with a sample of the initial anorthosite in the amount of 25–40 mg, a sample of NaCl ± oxalic acid, and then distilled water was poured in. The ampoules were filled with excess fluid relative to the rock. After filling, the ampoules were welded, turned over and shaken well to distribute the components more evenly. All experiments were conducted in gold ampoules to avoid iron losses. Oxygen volatility was not controlled and was taken to be close to the Ni-NiO buffer (Helz, 1976). The experiments lasted four days, after which they were quenched.

After the experiments, the solid component of the products was washed from excess salt and glued with epoxy resin to a glass plate, then polished to a thickness of 0.5-2 mm. The compositions of mineral phases were studied by the method of local X-ray spectral microanalysis using scanning electron microscopes CamScan MV2300 (VEGA TS 5130MM) and Tescan VEGA-II XMU, equipped with energy-dispersive spectrometers INCA Energy 450, at an accelerating voltage of 20 kV, a beam current of 150–400 pA, and a spectrum acquisition time of 70 sec.

Results of experiments. Table 1 shows the compositions of the fluid phase and the main mineral associations after the experiments. With the given parameters, amphibole and quenched melt are the main phases after the experiments, regardless of the fluid composition (Fig. 1). Clino- and orthopyroxenes were not detected in the experiments with low salt contents (experiment 5-IS). With increasing salinity of the solutions, pyroxenes are preserved only in the form of remaining small grains surrounded by amphibole (Fig. 1a), i.e. they also become unstable.

Table 1. Composition of the initial fluid in the ampoules and phases after the experiments

Run numb.:	The composition of the fluid	Post-experiment phases	Remarks
2Z	There is no fluid	*Opx*+*Pl*+*Cpx*+FeS	
H_2O-NaCl Fluid			
6-IS	H_2O	Hbl_1+Hbl_2+Hbl_3 +*Gl*+*Chl*	
5-IS	X_{NaCl} =0.07	Hbl_1+Hbl_2+ *Gl*+*Chl*	
5Z	X_{NaCl} = 0.10	*Gl*+Hbl_1+Hbl_2+*Hbl*+ (Fe_3O_4 x $V_{0.44}O_{1.32}$)	anorthosite + 1 wt.% TiO_2 and V_2O_3 and 3.4 wt.% FeO
3-IS	X_{NaCl} = 0.17	Hbl_1+Hbl_2+*Cpx*+Hbl_3+*Gl*+*Ilm*	
4-IS	X_{NaCl} = 0.36	Hbl_1+Hbl_2+Hbl_3+*Cpx*+*Gl*+*Ilm*+*Rt*	
3K	X_{NaCl} = 0.50	*Ilm*+*Cpx*+Hbl_1+Hbl_2+Hbl_3+*Gl*	
2K	X_{NaCl} = 0.63	*Cpx*+ Hbl_1 + Hbl_2 + Hbl_3 + *Gl*	

Run numb.:	The composition of the fluid	Post-experiment phases	Remarks
H_2O-NaCl-CO_2 Fluid			
1-IS	X_{NaCl} = 0.17 X_{H2O} = 0.60 X_{CO2} = 0.23	*Hbl_1+Hbl_2+ Gl+Cal+Chl*	
2-IS	X_{NaCl} = 0.33 X_{H2O} = 0.33 X_{CO2} = 0.34	*Hbl_1+Hbl_2+ Gl+Cal+Cpx+Opx*	

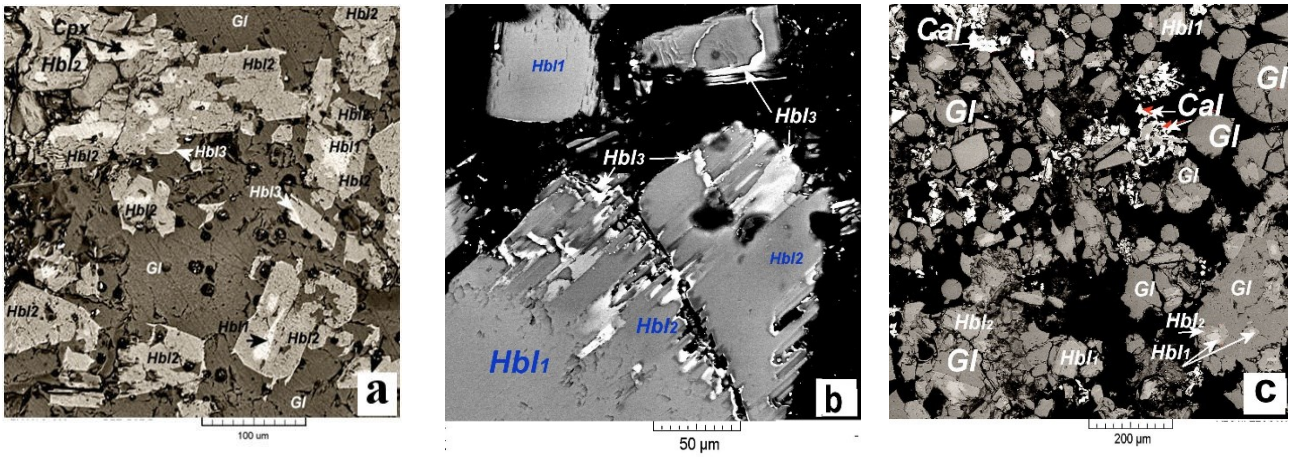

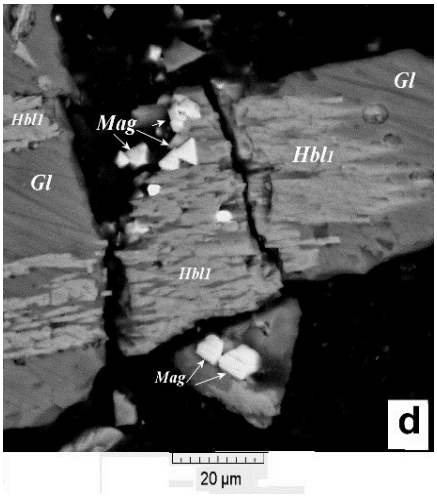

Fig. 1. BSE photographs of the experimental products: (a) large and zoned amphiboles with lighter areas in the center *(Hbl_1)* and darker ones at the edges *(Hbl_2),* quenched melt between amphiboles (experiment 4-IS); (б) – unequal distribution of Fe - Mg in amphibole with the formation of highly-Fe *Hbl_3*, (experiment 5-IS); (в) – tiny carbonates between spherical forms of quenched melt and amphiboles (experiment 1-IS); (d) –.(г) – crystals of newly formed magnetite in experiment 5Z.

In Fig. 1 it is evident that zoning with a lighter – ferruginous – composition in the center (*Hbl_1*) and more magnesian edges (*Hbl_2*) is observed in large amphibole crystals. In almost all experiments, light areas (*Hbl_3*) are observed at the very edges of the amphibole, as well as along cracks and cleavage planes (Fig. 1b). The melt occupies interstices between idiomorous amphiboles (Fig. 1a) or is concentrated in the form of spherical formations (Fig. 1c). The appearance of such spherical forms is a characteristic feature of experiments on melting aluminosilicates in water-salt solutions due to the fact that the two liquids (melt and fluid) are not wetted (Newton, Manning, 2008, etc.).

In experiment 5Z (Table 1), in which a mixture of TiO_2 -V_2O_3 -FeO was added to the initial sample, very small, less than 5 µm, rectangular crystals appeared after the experiment (Fig. 1g). This is newly formed magnetite, the average composition of which is: Fe_3O_4 x.$V_{0.44}O_{1.32}$.

Ilmenite after the experiments was represented by very rare crystals or even their absence in the samples after the experiments. This is due to the fact that the content of ilmenite in the initial anorthosite is small, so it could not get into the initial sample of anorthosite placed in the ampoule.

In experiments with H_2O-NaCl-CO_2 fluid, melt and zonal amphibole *Hbl_1* and *Hbl_2* were noted, however, *Hbl_3* were not noted, the removed iron was bound with CO_3^{2-} anions, forming small, unevenly

distributed carbonates $(Ca_{0.23}Fe_{0.77})CO_3$ - $(Ca_{0.28}Fe_{0.72})CO_3$ (Fig. 1c).

Composition of phases after experiments

Melts. The composition of the resulting melts in the H_2O-NaCl system is characterized by a decrease in the SiO_2 and CaO content and an unchanged Al_2O_3 content with increasing fluid salinity (Table 2). In the H_2O-NaCl-CO_2 system, the Ca and Fe content in the melt is lower by ≈1-2% due to the precipitation of carbonates. The TiO_2 content in the melts is 0-0.3%, and is practically independent of X_{NaCl}. However, adding TiO_2 to the initial sample leads to an increase in the TiO_2 content in the melt to 1.1% (run 5Z in Table 1). The FeO content varies in the range of 0-4% and does not change when adding 3% FeO to the initial sample; the dependence on X_{NaCl} is also not obvious.

Table 2. Average values of oxide content (wt%) of quenched melts (normalized to 100%)

Run no.:	5-IS	5Z	3-IS	4-IS	3K
	X_{NaCl} =0.07	X_{NaCl} = 0.10	X_{NaCl} =0.17	X_{NaCl} =0.36	X_{NaCl} = 0.50
SiO_2	62.422	64.23	62.745	58.69	58.68
TiO_2	0.144	0.70	0.07	0.365	0.02
Al_2O_3	22.24	21.45	21.125	22.12	23.14
FeO	2.215	2.34	3.04	2.88	1.70
MnO	0.058	0.08	0	0.05	0.08
MgO	0.589	0.59	1.045	1.31	0.59
CaO	7.354	3.25	5.37	3.67	2.07
Na_2O	4.405	6.87	5.79	9.44	12.15
K_2O	0.208	0.21	0.14	0.22	0.07
Cl_2O	0.378	0.32	0.89	1.28	1.48

The Cl content in the melt increases with increasing X_{NaCl} in the fluid, and the Cl content in the melt in the case of a homogeneous aqueous-chloride fluid is somewhat lower than in the presence of a two-phase H_2O-NaCl-CO_2, which has already been noted (Chevychelov, 2006).

In general, with an increase in X_{NaCl} in the initial fluid, the composition of the melts changes from diorites and granodiorites to syenites. In the H_2O-NaCl-CO_2 system, the composition of the melts is characterized by a slightly higher content of SiO_2 and alkalis and corresponds not to diorites, but to quartz monzonites.

Amphiboles

The amphiboles formed in the experiments belong to the group of calcium ones, in which $(Ca+Na)_B > 1.50$ and $Na_B < 0.50$, are close to pargasites (Leake et al., 1997). The compositions (Hbl_1) are characterized by the iron content f_{Hbl1} = 0.3-0.4 in the center. The alkali content in Hbl_1 $(Na+K)_{Hbl1}$ increases with increasing X_{NaCl} in the fluid. Hbl_1 from the center to the edges is replaced by magnesian Hbl_2, the iron content of which is $f < 0.2$. This indicates the removal of Fe and its redeposition at the very edges of the mineral, Hbl_3 are formed, the iron content of which is close to 1 (Hbl_1 - Hbl_2 - Hbl_3 in Fig. 1b). Only Hbl_1 amphiboles obtained in the experiments are close in composition to amphiboles in natural metasomatic veins.

The maximum content of TiO_2 in amphibole Hbl_1 from the experiments is also close to its content in natural metasomatic amphiboles, as is FeO. In the middle and marginal parts of amphibole (respectively Hbl_2 and especially Hbl_3) TiO_2 is almost absent, i.e. Ti, as well as Fe, is removed from amphibole.

Ilmenite

The initial ilmenite changes its composition after the experiments. As can be seen in Fig. 2, with an increase in X_{NaCl}, the TiO_2 content in ilmenite slightly increases and FeO decreases in the fluid. The MgO content in the mineral increases sharply with an increase in salinity and already at $X_{NaCl} > 0.17$ is about 10%, which is not typical for most industrial ilmenite concentrates, in which the MgO content is usually: 0.1–2.0% (most often 0.5–1.5%). However, if the iron removed from the amphibole is fixed either in the form of Hbl_3 or in the form of ferrous carbonates, it remains unclear due to which elements the changes in the ilmenite composition occur: most likely due to the removal of FeO with the subsequent formation of magnetite. However, it is possible that in the experiments the increase in the TiO_2 content in ilmenite (Fig. 2) occurred due to Ti removed from Hbl_2 and Hbl_3.

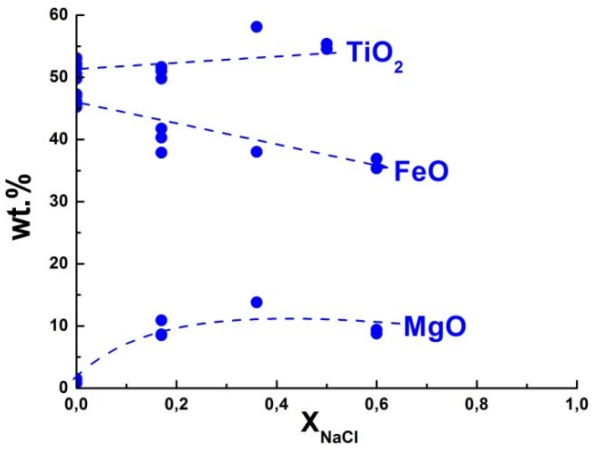

Fig. 2. The content of MgO, FeO, and TiO_2 in ilmenite after experiments with various X_{NaCl} in the fluid.

Conclusion. The results of the experiments showed that the interaction of H_2O-NaCl solutions with anorthosites results in the formation of *Hbl*$_1$ amphiboles - pargasites, the composition of which fully corresponds to the compositions of amphiboles in natural melanocratic veins. With a decrease in aH_2O caused by an increase in X_{NaCl} and/or the addition of X_{CO2} to the fluid composition, clino-orthopyroxenes can be preserved in the experimental products (Table 1). The normative composition of the obtained melts includes acid plagioclases, sometimes present in natural mafic veins. The mineral associations obtained in the experiments, mainly pargasite, acid plagioclase, and the remaining anorthosite minerals - clino- and orthopyroxenes, correspond in composition to the corresponding minerals of melanocratic veins. However, the appearance of ferrous carbonates in the case of interaction of anorthosites with H_2O-NaCl±CO_2 fluids is not typical for melanocratic veins. Only during retrograde recrystallization of veins at the cooling stage are very thin secondary reaction *Hbl* - or *Hbl-Pl* borders between *Grt* and *Mag* grains often observed, as well as the thinnest *Hbl±Bt±Ttn* veinlets, sometimes with calcite, steeply intersecting the linearity of the veins (Khodorevskaya, Korikovsky, 2007).

In experiments, it was found that Fe and Ti are removed from mafic anorthosite minerals. A clear removal of Fe was noted in the formation of *Hbl*$_3$ and carbonates with a high Fe content. A decrease in the TiO_2 content from the centers to the edges of the amphibole was also observed. However, newly formed Fe-Ti minerals were not noted. And only with the addition of small amounts of TiO_2, V_2O_3 and FeO to the initial anorthosite sample, magnetite appeared and the TiO_2 content in the melt increased (experiment 5Z), but newly formed ilmenite was not observed even with the addition of TiO_2.

Thus, the experiments conducted confirmed the statement that the formation of high-temperature melanocratic veins in gabbro-anorthosites occurs at high P-T parameters with the participation of fluids of complex composition, in which, along with H_2O and CO_2, highly concentrated solutions and brines of salts play a large role. However, we did not obtain the conditions for the localization or concentrated redeposition of ilmenite-magnetite, as is observed in the internal zones of natural metasomatic melanocratic veins. Further experimental studies are necessary for this.

Funding. The work was carried out within the framework of the research project of the IEM RAS No. FMUF-2022-0004.

References

Bogdanova M. N., Efimov M. M., Sorokhtin R. O., et al., Development of the Polymetamorphism in the Granulite Belt of the Kola Peninsula (Kolvitsa Zone), and U–Pb Dating the Diaphthoresis of the Anorthosite Association// Dokl. Akad. Nauk. 1993. V. 331. № 1. P. 95–98.

Korikovsky S. P., Aranovich L. Ya. Charnockitization and Enderbitization of Mafic Granulites in the Porya Bay Area, Lapland Granulite Belt, Southern Kola Peninsula: I. Petrology and Geothermobarometry// Petrology. 2010. V. 18. P. 320–349.

Khodorevskaya L. I., Korikovskii S. P. Metasomatic Garnet–Clinopyroxene–Orthopyroxene–Hornblende Veins in Metaanorthosites of the Kolvitsa Massif, Kola Peninsula: Mineral Composition and Relation with Syngranulite Granitization //Dokl. Earth Sci. 2007. V. 415A. P. 915–918.

Khodorevskaya L.I. Granulite facies metamorphism and metasomatism in the gabbro-anorthosites of the Kolvitsa massif, Kola peninsula// Geochemistry International. 2012. V. 50, № 3. P. 272-288.

Chevychelov V.Yu., Distribution of volatiles, rock-forming, and ore components in the magmatic systems: experimental studies, Extended Abstract of Doctoral (Geolmin) Dissertation, Moscow: MGU, 2013.

Helz R. T. Phase relations of basalts in their melting ranges at P_{H2O} = 5 kb. Part II. Melt compositions //Journal of Petrology. – 1976. – T. 17. – №. 2. – C. 139-193. https://doi.org/10.1093/petrology/17.2.139

Leake B. E. Nomenclature of amphiboles //Mineralogical Magazine. – 1997. – T. 61. – C. 296-311.

Newton R.C., Manning C.E. Solubility of corundum in the system Al_2O_3–SiO_2–H_2O–NaCl at 800°C and 10 kbar // Chem. Geol. 2008. V. 249. P. 250–261.

Shornikov S. I. Thermodynamic properties of the Li_2O–SiO_2 melts.

V. I. Vernadsky Institute of Geochemistry & Analytical Chemistry RAS, Moscow sergey.shornikov@gmail.com

Abstract. The thermodynamic properties of the Li_2O–SiO_2 melts in the temperature region 1000–2000 K were calculated within the framework of the developed semi-empirical model. The calculated partial pressures of vapor species as well as the oxide activities and the mixing energies of melts are compared with available information.

***Keywords**: thermodynamic properties of oxide melts, the Li_2O–SiO_2 system*

The physicochemical properties of lithium silicates and their melts are of considerable interest for the production of ceramics and lacquers, in construction, as well as in other branches of modern industry (Tulyaganov et al., 2025). It is assumed that lithium isotopes can potentially reveal the role of liquid water in the early Solar system (Sephton et al., 2013).

The following lithium silicates have been found in the Li_2O–SiO_2 system: Li_4SiO_4 ($2Li_2O \cdot SiO_2$), Li_2SiO_3 ($Li_2O \cdot SiO_2$) and $Li_2Si_2O_5$ ($Li_2O \cdot 2SiO_2$), which melt congruently at 1528, 1474, and 1307 K. The compound of Li_8SiO_6 ($4Li_2O \cdot SiO_2$) decomposes at 1104 K, the compound of $Li_6Si_2O_7$ ($3Li_2O \cdot 2SiO_2$) exists in a limited temperature range of 1493–1503 K. Lithium silicates of $Li_2Si_3O_7$ ($Li_2O \cdot 3SiO_2$) and $Li_4Si_3O_8$ ($2Li_2O \cdot 3SiO_2$) dissociate at temperatures not exceeding 600 K (Takahashi and Yoshio, 1970). The high-temperature region of phase relations in the Li_2O–SiO_2 system is shown in Fig. 1 (Claus et al., 1996; Lee et al., 2025).

The few data on the enthalpies of formation and phase transitions, as well as the temperature dependences of the Li_4SiO_4, Li_2SiO_3 and $Li_2Si_2O_5$ heat capacities, are reviewed in (Barin, 1995; Konar et al., 2017; De Abreu, Fabrichnaya 2024). The partial pressures of Li, LiO, Li_2O, Li_3O, SiO, O_2 and Li_2SiO_3 identified in the vapor over Li_2SiO_3 (Nakagawa et al., 1981; Ikeda et al., 1982; Penzhorn et al., 1988; Asano and Nakagawa, 1989) and Li_4SiO_4 (Ikeda et al., 1982; Ihle et al., 1989), were determined by mass spectrometry during the melt evaporation from Knudsen effusion platinum cells in the temperature range of 1100–1900 K. As follows from Fig. 2, the results obtained differ by an order of magnitude and contain significant errors.

Schultz et al. (1986) determined the lithium oxide activities in the Li_2O–SiO_2 melts in the compositions range compositions from 50 to 90 mol % SiO_2 by the EMF method at 1173–1473 K (Fig. 3A). The thermodynamic properties of the melts were calculated taking into account the normalization of experimental data to those for Li_2SiO_3 lithium metasilicate reference. Previously obtained by mass spectrometry (Ikeda et al., 1982) the lithium oxide activities in Li_4SiO_4 and Li_2SiO_3 at 1600 K did not contradict these results (Fig. 3A).

The calculations of the thermodynamic properties of the Li_2O–SiO_2 melts in the temperature range of 1000–2000 K were performed in the present study using a semi-empirical model (Shornikov, 2019). The model parameters were the standard Gibbs energies ($\Delta G°$) values calculated from experimental and theoretical data for the formation of simple oxides (Li_2O and SiO_2) and lithium silicates (Li_8SiO_6, Li_4SiO_4, Li_2SiO_3, $Li_6Si_2O_7$ and $Li_2Si_2O_5$). The standard Gibbs energy initial values for the formation of simple oxides in the crystalline and liquid states, as well as information on possible equilibria in the gas phase over the melt involving atomic and molecular species (Li, Li_2, LiO, Li_2O, Li_2O_2, Si, Si_2, Si_3, Si_4, SiO, SiO_2, Si_2O_2, Li_2SiO_3, O, O_2, O_3, and O_4) were adopted on reference data (Barin, 1995), as well as the experimental results obtained in (Nakagawa et al., 1981; Penzhorn et al., 1988). The $\Delta G°$ values of the condensed phases and the vapor species over the melt were used to find the equilibrium conditions for a given melt composition and temperature.

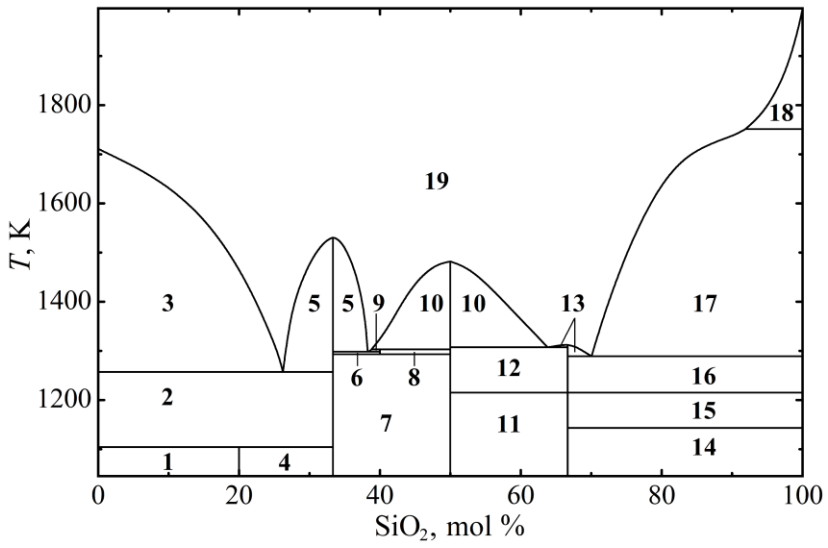

Fig. 1. The phase relations in the Li_2O–SiO_2 system: 1 – Li_2O + Li_8SiO_6; 2 – Li_2O + Li_4SiO_4; 3 – Li_2O + liquid; 4 – Li_8SiO_6 + Li_4SiO_4; 5 – Li_4SiO_4 + liquid; 6 – Li_4SiO_4 + $Li_6Si_2O_7$; 7 – Li_4SiO_4 + Li_2SiO_3; 8 – $Li_6Si_2O_7$ + Li_2SiO_3; 9 – $Li_6Si_2O_7$ + liquid; 10 – Li_2SiO_3 + liquid; 11 – Li_2SiO_3 + α-$Li_2Si_2O_5$; 12 – Li_2SiO_3 + β-$Li_2Si_2O_5$; 13 – β-$Li_2Si_2O_5$ + liquid; 14 – α-$Li_2Si_2O_5$ + SiO_2 (β-quartz); 15 – α-$Li_2Si_2O_5$ + SiO_2 (tridymite); 16 – β-$Li_2Si_2O_5$ + SiO_2 (tridymite); 17 – SiO_2 (tridymite) + liquid; 18 – SiO_2 (cristobalite) + liquid; 19 – liquid.

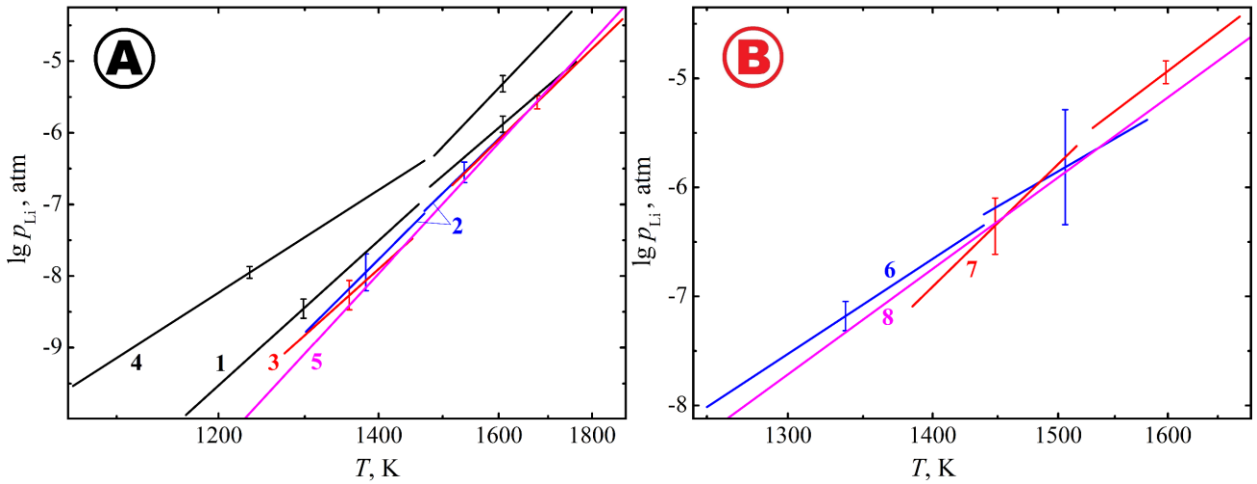

Fig. 2. Logarithm temperature dependence of the Li partial pressure vapor specie over Li_2SiO_3 (A) and Li_4SiO_4 (B), determined by mass spectrometry in (Nakagawa et al., 1981; Asano, Nakagawa, 1989) (1, 4), (Ikeda et al., 1982) (2, 6), (Penzhorn et al., 1988; Ihle et al., 1989) (3, 7), as well as calculated in the present study (5, 8).

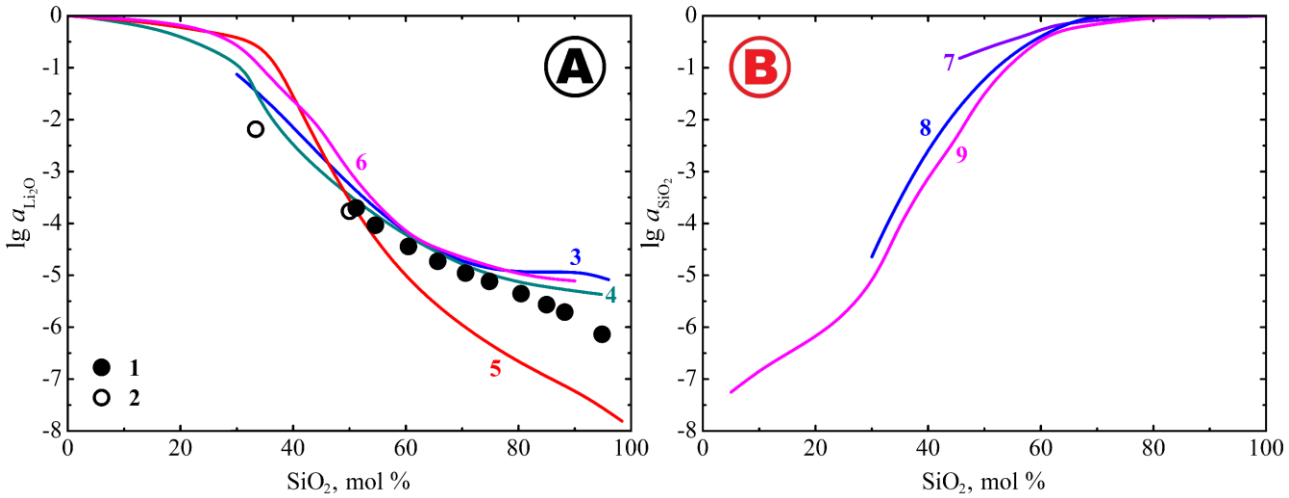

Fig. 3. The Li_2O (A) and SiO_2 (B) activities in the Li_2O–SiO_2 melts determined by the EMF method in (Schultz et al., 1986) at 1473 K (1) and by the mass spectrometric method in (Ikeda et al., 1982) at 1600 K (2), as well as calculated in (Charles, 1967) (3, 8), (Konar et al., 2017) (4), (De Abreu, Fabrichnaya, 2024) (5), (Callow, 1950) (7), and in the present study (6, 9) at 1600 (1) and 1673 (2–8) K.

The calculations of Li_2O activities in the Li_2O–SiO_2 melts at 1673 K (Fig. 3A) correspond to experimental data (Ikeda et al., 1982; Schultz et al., 1986) obtained at lower temperatures (1473 and 1600 K) and coincide with those calculated in (Charles, 1967; Konar et al., 2017). The Li_2O calculated activities in (De Abreu, Fabrichnaya, 2024) in the composition range from 50 to 95 mol % SiO_2 is significantly lower than the experimental data obtained at lower temperatures, as well as than the results of other calculations performed at the same temperature.

The SiO_2 activity (Fig. 3B) in lithium-silicate melts has not been experimentally determined. The calculated values in the present study are close to the results obtained in (Charles, 1967). The calculations in (Callow, 1950) differ significantly from them and do not correspond to the available experimental data on the Li_2SiO_3 melts (Barin, 1995).

Further calculation of the partial pressures of the vapor species over the Li_2SiO_3 and Li_4SiO_4 melts showed satisfactory agreement with the available data obtained by the mass spectrometric method. Fig. 2 illustrates this agreement for the case of the temperature dependence of the partial pressure of Li (the predominant specie of the gas phase over lithium meta- and orthosilicates): the p_{Li} calculated values are close to the experimental values obtained in (Nakagawa et al., 1981; Ikeda et al., 1982; Penzhorn et al., 1988; Ihle et al., 1989).

The calculated values of the mixing energies in the Li_2O–SiO_3 melts at 1673 K (Fig. 4) coincide with those calculated in (Charles, 1967) and correspond to the sequence of chemical interaction in alkali-silicate melts: Li_2O–SiO_2 → Na_2O–SiO_2 → K_2O–SiO_2.

Thus the thermodynamic properties of the Li_2O–

SiO_2 melts are calculated in the temperature range of 1000–2000 K in the present study. The obtained partial pressures of the vapor species over the melt, as well as the oxide activities and mixing energies in the melts correspond to the available experimental and theoretical information.

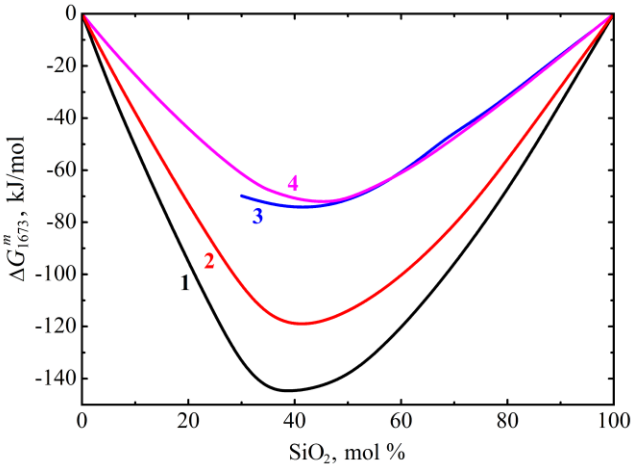

Fig. 4. The mixing energy in the K_2O–SiO_2 (1), Na_2O–SiO_2 (2), and Li_2O–SiO_2 (3, 4) melts calculated in (Shornikov, 2013) (1), (Shornikov, 2014) (2), (Charles, 1967) (3) and in the present study (4) at 1673 K.

Financing: The study was performed within the framework of the state assignment of the Vernadsky Institute of Geochemistry & Analytical Chemistry of the Russian Academy of Sciences.

References

Asano M., Nakagawa H. (1989) Vaporization of lithium metasilicate in a graphite Knudsen cell. *J. Nucl. Mater.*, vol. 161, № 2, pp. 190–196.

Barin I. (1995) Thermochemical data of pure substances. Weinheim, VCH, 2003 p.

Callow R. J. (1950) Activities in alkali oxide – silica melts. *Trans. Faraday Soc.*, vol. 46, № 8, pp. 663–673.

Charles R. J. (1967) Activities in Li_2O–, Na_2O–, and K_2O–SiO_2 solutions. *J. Amer. Ceram. Soc.*, vol. 50, № 12, pp. 631–641.

Claus S., Kleykamp H., Smykatz-Kloss W. (1996) Phase equilibria in the Li_4SiO_4–Li_2SiO_3 region of the pseudobinary Li_2O–SiO_2 system. *J. Nucl. Mater.*, vol. 230, № 1, pp. 8–11.

De Abreu D. A., Fabrichnaya O. (2024) Critical experiments and thermodynamic modeling of the Li_2O−SiO_2 system. *Solids*, vol. 5, № 2, pp. 303–320.

Ihle H. R., Penzhorn R. D., Schuster P. (1989) The thermochemistry of lithium silicates in view of their use as breeder materials. *Fusion Engineering & Design*, vol. 8, pp. 393–397.

Ikeda Y., Tamaki M., Matsumoto G., Amioka K., Mizuno T. (1982) Mass spectrometric studies of lithium-containing oxides at high temperature. *Spectrochim. Acta B*, vol. 37, № 8, pp. 647–658.

Konar B., Van Ende M. A., Jung I. H. (2017) Critical evaluation and thermodynamic optimization of the Li–O, and Li_2O–SiO_2 systems. *J. Eur. Ceram. Soc.*, vol. 37, № 5, pp. 2189–2207.

Lee J., Lauriano P., Jung I. H. (2025) Liquidus of SiO_2 in the Li_2O–SiO_2, Na_2O–SiO_2, and K_2O–SiO_2 systems. *J. Amer. Ceram. Soc.*, vol. 108, № 3, p. e20255.

Nakagawa H., Asano M., Kubo K. (1981) Mass spectrometric study of the vaporization of lithium metasilicate. *J. Nucl. Mater.*, vol. 102, № 3, pp. 292–297.

Penzhorn R. D., Ihle H. R., Schuster P., Zmbov K. (1988) The evaporation process of solid lithium metasilicate. *J. Nucl. Mater.*, vol. 155, pp. 471–475.

Sephton M. A., James R. H., Fehr M. A., Bland P. A., Gounelle M. (2013) Lithium isotopes as indicators of meteorite parent body alteration. *Met. & Planet. Sci.*, vol. 48, № 5, pp. 872–878.

Shornikov S. I. (2013) Thermodynamic properties of the K_2O–SiO_2 melts. *Experiment in Geosciences*, vol. 19, № 1, pp. 108–111.

Shornikov S. I. (2014) Thermodynamic properties of sodium-silicate melts. *Experiment in Geosciences*, vol. 20, № 1, pp. 48–51.

Shornikov S. I. (2019) Thermodynamic modelling of evaporation processes of lunar and meteoritic substance. *Geochem. Int.*, vol. 57, № 8, pp. 865–872.

Shultz M. M., Kozhina E. L., Shakhmatkin B. A. (1986) Thermodynamic properties of Li_2O–SiO_2 melts. *Vestnik LGU*, ser. 4, № 1, pp. 55–60 [in russian].

Tulyaganov D. U., Alves M. F., Dimitriadis K., Murtazaev S., Agathopoulos S., Fernandes H. R. (2025) Fundamentals and advances in production and application of non-stoichiometric lithium disilicate glass-ceramics: a brief review. *Ceram. Int.*, vol. 51, № 12A, pp. 15067–15076.

Shornikov S.I. Thermodynamic properties of the Li_2O–P_4O_{10} melts.

V. I. Vernadsky Institute of Geochemistry & Analytical Chemistry RAS, Moscow sergey.shornikov@gmail.com

Abstract. Calculations of the thermodynamic properties of Li_2O–P_4O_{10} melts in the temperature range of 700–1800 K were carried out for the first time within the framework of the developed semi-empirical model. A comparison of the calculated oxide activities and the mixing energy in the Li_2O–P_4O_{10} melts confirms the typical rules characteristic of potassium- and sodium-phosphate melts.

***Keywords**: thermodynamic properties of oxide melts, the Li_2O–P_4O_{10} system*

The physico-chemical properties of lithium phosphates and their melts are of considerable interest for the production of lithium-ion batteries with increased safety and cyclic stability.

The Li_2O–P_4O_{10} system contains $LiPO_3$ ($2Li_2O \cdot P_4O_{10}$), $Li_4P_2O_7$ ($4Li_2O \cdot P_4O_{10}$) and lithium phosphate Li_3PO_4 ($6Li_2O \cdot P_4O_{10}$), which melt congruently at temperatures of 938, 1158 and 1498

K. The last two lithium phosphates exist in various structural modifications depending on the temperature. The literature also mentions compounds $Li_5P_3O_{10}$ ($10Li_2O \cdot 3P_4O_{10}$) and $Li_6P_4O_{13}$ ($3Li_2O \cdot P_4O_{10}$) dissociating at temperatures not exceeding 400 K (Meadowcroft, Richardson, 1963). One of the variants of the Li_2O–P_4O_{10} phase diagram in the high-temperature region is shown in Fig. 1 (Xie et al., 2020).

Few experimental data on the thermodynamic properties of $LiPO_3$, $Li_4P_2O_7$ and Li_3PO_4 have been reviewed (Ong et al., 2008; Jin et al., 2019; Xie et al., 2020). Note that the estimated values of the mixing enthalpies of these compounds at 298 K are in a rather narrow range from –272 to –255 kJ/mol (Wagman et al., 1981).

Like other K_2O–P_4O_{10} (Shornikov, 2024) and Na_2O–P_4O_{10} (Shornikov, 2024a) alkaline phosphate melts, the Li_2O–P_4O_{10} melt evaporation occurs with the formation of gaseous metaphosphate (Ratkovsky et al., 1974, 1976; Alikhanyan et al., 1975; Steblevsky et al., 1977, 1978) according to the reaction:

$$[LiPO_3] = (LiPO_3) \quad (1)$$

(condensed and gaseous phases are indicated in square and round brackets). These molecules subsequently dissociate to form vapor species – (Li), (LiO), (Li_2O), (P), (P_2), (PO), (PO_2), (PO_3), and (O_2), as well as the ($Li_2P_2O_6$) dimer. As follows from Fig. 1, the dependences of the $LiPO_3$ partial pressure over the $LiPO_3$ melt on the reverse temperature obtained in these experimental studies are consistent with each other within the error limits.

The calculations of the oxide activities in the Li_2O–P_4O_{10} melts in the temperature range 700–1800 K were performed in the present study for the first time within the framework of the developed semi-empirical model (Shornikov, 2019). The model parameters were the standard Gibbs energies values ($\Delta G°$) calculated from experimental and theoretical data on the formation of simple oxides (Li_2O and P_4O_{10}) and lithium phosphates (Li_3PO_4, $Li_4P_2O_7$, $Li_5P_3O_{10}$, $Li_6P_4O_{13}$, $LiPO_3$). The initial values of the standard Gibbs energies on the formation of simple oxides in the crystalline and liquid states, as well as information on possible equilibria in the gas phase over the melt involving atomic and molecular forms (Li, Li_2, LiO, Li_2O, Li_2O_2, P, P_2, P_3, P_4, PO, PO_2, PO_3, P_2O_3, P_2O_4, P_2O_5, P_3O_6, P_4O_6, P_4O_7, P_4O_8, P_4O_9, P_4O_{10}, O, O_2, O_3, O_4, and $LiPO_3$) were adopted on reference data (Glushko, 1978–1982; Barin, 1995), as well as the results obtained by Ratkovsky et al. (1974). The $\Delta G°$ values of the condensed phases and the vapor species over the melt were used to find the equilibrium conditions for a given melt composition and temperature.

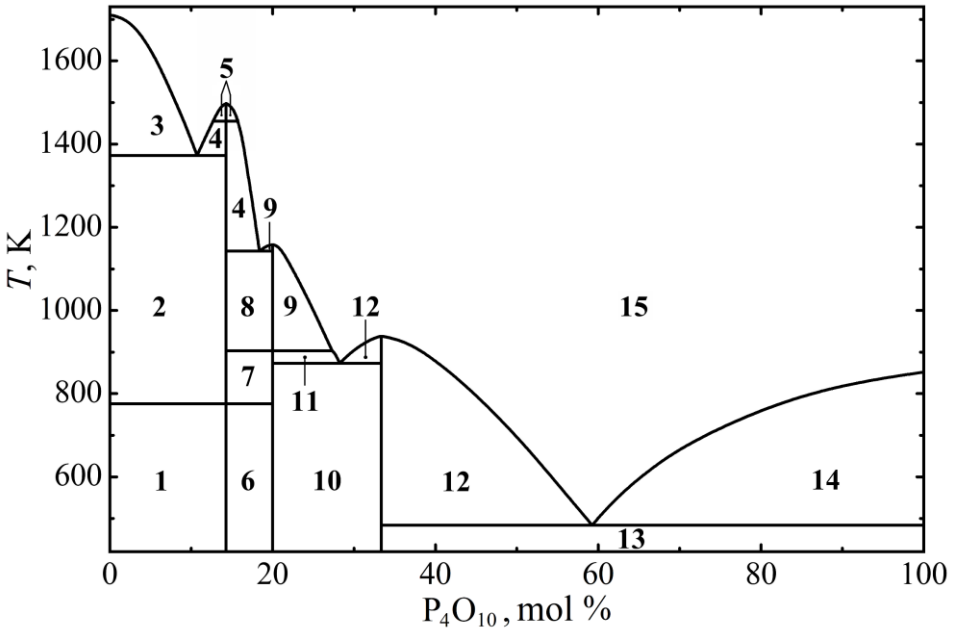

Fig. 1. The phase diagram of the Li_2O–P_4O_{10} system: 1 – Li_2O + α-Li_3PO_4; 2 – Li_2O + β-Li_3PO_4; 3 – Li_2O + liquid; 4 – β-Li_3PO_4 + liquid; 5 – γ-Li_3PO_4 + liquid; 6 – α-Li_3PO_4 + α-$Li_4P_2O_7$; 7 – β-Li_3PO_4 + α-$Li_4P_2O_7$; 8 – β-Li_3PO_4 + β-$Li_4P_2O_7$; 9 – β-$Li_4P_2O_7$ + liquid; 10 – α-$Li_4P_2O_7$ + $LiPO_3$; 11 – α-$Li_4P_2O_7$ + liquid; 12 – $LiPO_3$ + liquid; 13 – $LiPO_3$ + P_4O_{10}; 14 – P_4O_{10} + liquid; 15 – liquid.

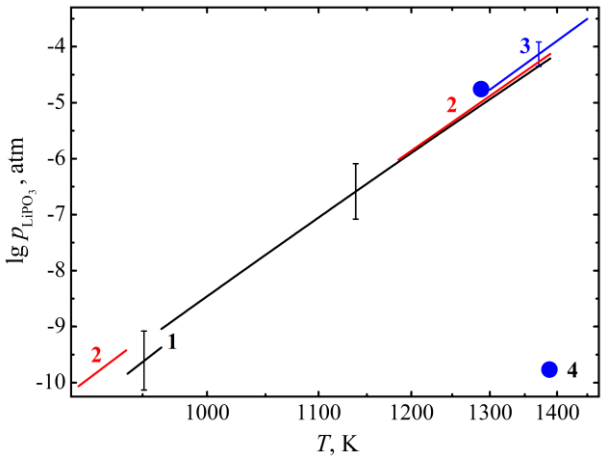

Fig. 2. The temperature dependence of the logarithm of $LiPO_3$ partial pressure in the vapor over the $LiPO_3$ melt determined by the mass spectrometric method in (Ratkovsky et al., 1974, 1976) (1, 2), (Alikhanyan et al., 1975; Steblevsky et al., 1977) (3, 4).

A comparison of calculations of the oxide activities and mixing energy in the Li_2O–P_4O_{10} melts at 1673 K obtained in the present study with those for the K_2O–P_4O_{10} (Shornikov, 2024) and Na_2O–P_4O_{10} (Shornikov, 2024a) melts shows typical rules characteristic of alkaline melts (Fig. 3). Fig. 3A shows a certain closeness of the concentration dependences of the P_4O_{10} activities, and a symmetrical decrease in the alkaline oxide activity in the series: Li_2O → Na_2O → K_2O. The observed characteristic dependence is determined by the sequence of chemical interaction in alkali-phosphate melts, as can be seen from Fig. 3B. The minimum values of mixing energies in melts are in a wide range of concentrations from 22 to 27 mol % P_4O_{10}, due to the proximity values of the mixing enthalpies of meta- and orthophosphates, as well as low values of their mixing entropies.

Thus, the thermodynamic properties of the Li_2O–P_4O_{10} melts in the temperature range of 700–1800 K are calculated in the present study for the first time. A comparison of the calculated values of the oxide activities and the mixing energy in the Li_2O–P_4O_{10} melts confirms the typical rules characteristic of potassium- and sodium-phosphate melts.

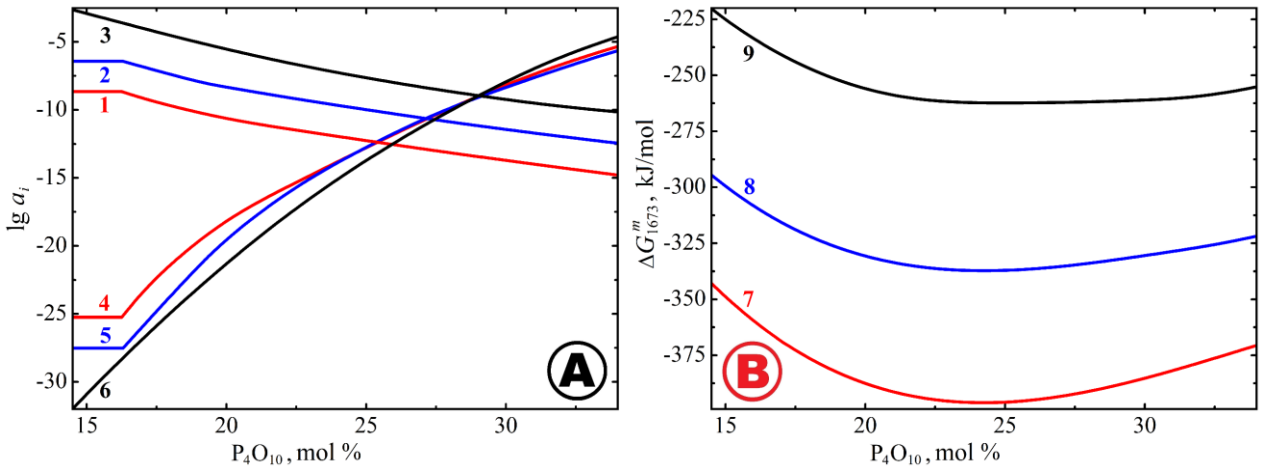

Fig. 3. The oxide activities (A) and the mixing energies (B) in the K_2O–P_4O_{10} (1, 4, 7), Na_2O–P_4O_{10} (2, 5, 8) and Li_2O–P_4O_{10} (3, 6, 9) melts, calculated in (Shornikov, 2024) (1, 4, 7), (Shornikov, 2024a) (2, 5, 8) and in the present study (3, 6, 9) at 1673 K.

Financing: The study was performed within the framework of the state assignment of the Vernadsky Institute of Geochemistry & Analytical Chemistry of the Russian Academy of Sciences.

References

Alikhanyan A. S., Steblevsky A. V., Gorgoraki V. I., Sokolova I. D. (1975) Thermodynamic properties of alkali metal metaphosphates. *Doklady AN SSSR*, vol. 222, № 3, pp. 629–632.

Barin I. (1995) Thermochemical data of pure substances. Weinheim, VCH, 2003 p.

Glushko V. P., Gurvich L. V., Bergman G. A., Veitz I. V., Medvedev V. A., Khachkuruzov G. A., Yungman V. S. (1978–1982) Thermodynamic properties of individual substances. Moscow: Nauka.

Jin L., Wang J., Rousselot S., Dolle M., Chartrand P. (2019) Experimental and thermodynamic study of Li–O and Li_2O–P_2O_5 systems. *Can. J. Chem. Eng.*, vol. 97, № 8, pp. 2234–2241.

Meadowcroft T. R., Richardson F. D. (1963) Heats of formation of some crystalline and glassy phosphates. *Trans. Faraday Soc.*, vol. 59, № 7, pp. 1564–1571.

Ong S. P., Wang L., Kang B., Ceder G. (2008) Li–Fe–P–O_2 phase diagram from first principles calculations. *Chem. Mater.*, vol. 20, № 5, pp. 1798–1807.

Ratkovsky I. A., Krisko L. Y., Butylin B. A., Novikov G. I. (1974) Investigation of the vaporization process

of $LiPO_3$ using a mass spectrometer. *Doklady AN BSSR*, vol. 18, № 5, pp. 435–438.
Ratkovsky I. A., Ashuiko V. A., Urich V. A., Krisko L. Y. (1976) Energetics of formation of gaseous metaphosphates of alkali metals. *Izv. VUZ. Chem. & Chem. Technol.*, vol. 19, № 5, pp. 675–677.
Shornikov S. I. (2019) Thermodynamic modelling of evaporation processes of lunar and meteoritic substance. *Geochem. Int*., vol. 57, № 8, pp. 865–872.
Shornikov S. I. (2024) Thermodynamic properties of the K_2O–P_4O_{10} melts. *Experiment in Geosciences*, vol. 30, № 1, pp. 70–73.
Shornikov S. I. (2024a) Thermodynamic properties of the Na_2O–P_4O_{10} melts. *Experiment in Geosciences*, vol. 30, № 1, pp. 67–70.
Steblevsky A. V., Alikhanyan A. S., Sokolova I. D., Gorgoraki V. I. (1977) Thermal stability of alkali metal metaphosphates. *Russ. J. Neorg. Chem*., vol. 22, № 1, pp. 23–26.
Steblevsky A. V., Alikhanyan A. S., Sokolova I. D., Gorgoraki V. I. (1978) Thermodynamics of evaporation processes of sodium pyrophosphate and sodium and lithium orthophosphates. *Russ. J. Neorg. Chem*., vol. 23, № 2, pp. 309–315.
Wagman D. D., Evans W. H., Parker V. B., Schumm R. H., Nuttall R. L. (1981) Selected values of chemical thermodynamic properties. *U. S. NBS Technical Note* 270–8, 149 p.
Xie W., Wei S., Hudon P., Jung I.-H., Qiao Z., Cao Z. (2020) Critical evaluation and thermodynamic assessment of the R_2O–P_2O_5 (R = Li, Na and K) systems. *CALPHAD*, vol. 68, № 101718, 13 pp.